

## Time Point-Based Integrative Analyses of Deep-Transcriptome Identify Four Signal Pathways in Blastemal Regeneration of Zebrafish Lower Jaw

HUI ZHANG,<sup>a</sup> XUELONG WANG,<sup>a</sup> KAILUN LYU,<sup>a</sup> SIQI GAO,<sup>a</sup> GUAN WANG,<sup>b</sup> CHUNXIN FAN,<sup>a,c</sup>  
XIN A. ZHANG,<sup>d</sup> JIZHOU YAN<sup>a,c</sup>

**Key Words.** Zebrafish • Blastemal regeneration • foxi1 • RNA-sequencing • Tissue engineering

<sup>a</sup>Department of Biology, Institute for Marine Biosystem and Neurosciences, College of Fisheries and Life Sciences; and <sup>c</sup>Key Laboratory of Exploration and Utilization of Aquatic Genetic Resources Ministry of Education, Shanghai Ocean University Shanghai People's Republic of China; <sup>b</sup>Genergy Biotechnology (Shanghai) Co., Ltd., Shanghai, People's Republic of China; <sup>d</sup>Stephenson Cancer Center and Department of Physiology, The University of Oklahoma Health Sciences Center, Oklahoma City, Oklahoma, USA

Correspondence: Jizhou Yan, M.D., Ph.D., Institute for Marine Biosystem and Neurosciences, Department of Biology, College of Fisheries and Life Sciences, Ministry of Education, Shanghai Ocean University, Shanghai 201306, China. Telephone: 862161900488; Fax: 8621-61900445; e-mail: jyan2@shou.edu.cn

Received May 18, 2014; accepted for publication October 30, 2014; first published online in STEM CELLS EXPRESS November 25, 2014.

© AlphaMed Press  
1066-5099/2014/\$30.00/0

<http://dx.doi.org/10.1002/stem.1899>

### ABSTRACT

There has been growing interest in applying tissue engineering to stem cell-based regeneration therapies. We have previously reported that zebrafish can faithfully regenerate complicated tissue structures through blastemal cell type conversions and tissue reorganization. To unveil the regenerative factors and engineering arts of blastemal regeneration, we conducted transcriptomal analyses at four time points corresponding to preamputation, re-epitheliation, blastemal formation, and respecification. By combining the hierarchical gene ontology term network, the DAVID annotation system, and Euclidean distance clustering, we identified four signaling pathways: *foxi1-foxo1b-pou3f1*, *pax3a-mant3a-col11/col2*, *pou5f1-cdx4-kdrl*, and *isl1-wnt11 PCP-sox9a*. Results from immunohistochemical staining and promoter-driven transgenic fish suggest that these pathways, respectively, define wound epidermis reconstitution, cell type conversions, blastemal angiogenesis/vasculogenesis, and cartilage matrix-orientation. Foxi1 morpholino-knockdown caused expansions of Foxo1b- and Pax3a-expression in the basal layer-blastemal junction region. Moreover, foxi1 morphants displayed increased *sox9a* and *hoxa2b* transcripts in the embryonic pharyngeal arches. Thus, a Foxi1 signal switch is required to establish correct tissue patterns, including re-epitheliation and blastema formation. This study provides novel insight into a blastema regeneration strategy devised by epithelial cell transdifferentiation, blood vessel engineering, and cartilage matrix deposition. STEM CELLS 2015;33:806–818

### INTRODUCTION

Most invertebrate species, certain urodeles, and fish can faithfully regenerate their lost tissues and appendage organs, whereas most vertebrate species and mammals, including humans, do not have such regenerative capacity [1, 2]. Regenerative medicine aims to help humans restore the lost tissues, mostly through stem cell-based tissue engineering. Various stem cell types, including embryonic stem cells (ESCs), induced pluripotent stem cells (iPS), and adult stem cells, such as bone marrow mesenchymal stem cells and skin stem cells or epidermal neural crest stem cells (EPI-NCSC), are being investigated [3–6]. Immunogenicity of cell-based tissue replacement, the potential for teratoma or uncontrolled cell proliferation of ESC or iPS cells, and structural disorganization of stem cell components limit the clinical translation efficacy for such regenerative strategies.

Tissue engineering focuses on the construction of three-dimensional neotissues from their cellular components. Since angiogenesis is essential in almost all types of organ remodeling and

tissue engineering, devising blood vessel-engineered tissue becomes a challenge, particularly when designing a completely scaffold-free product [4]. One potential improvement involves the delivery of constructive cues to and modulation of the micro-environmental niche. Bioactive molecules could be used to spatially direct stem cell differentiation into multiple tissues [6]. Unfortunately, no such bioactive factors or biomaterials are well established. Thus, identifying the active factors and clarifying their interrelationships in distinct tissue niches from species with high tissue regeneration capabilities will aid in the identification and design of versatile biomaterials.

Zebrafish can faithfully regenerate complicated tissue structures. In our previous study [7], we described the regenerative process of the lower jaw and determined three time points that correspond to epidermis reconstruction, blastema formation, and reformation. Understanding the cellular and molecular pathways by which fish regenerate multiple tissue structures will help us to refine the regenerative rules for controlling proliferation and patterning in mammals and humans [8]. High-throughput transcriptomal analysis is an ideal approach to

identify the molecules which orchestrate the successive cell-type conversions, and provide regeneration mechanisms for tissue engineering or for induction of blastema regeneration. Although several papers have described the use of deep sequencing in animal regeneration studies [9–11], our study combined stereotyped cellular responses with time-lapse transcriptomic integrative analyses, and examined genotype-phenotype correlations that occur during the course of lower jaw regeneration.

## MATERIALS AND METHODS

### Zebrafish Husbandry

Zebrafish AB lines were maintained under an ambient temperature of 27°C with a timer-controlled light cycle of 14 hours light and 10 hours dark. All experiments were performed in accordance with the Animal Care and Use Committee guidelines of Shanghai Ocean University.

### Generation of Transgenic Fishes

Zebrafish *pou5f1* promoter-derived green fluorescent protein (GFP) expression construct pGFP-6.5 was a gift from Professor Kyo Yamasu. *Pou5f1:GFP* transgenic fish lines were generated as previously described [12]. *Flk1:GFP* and *Isl1:GFP* transgenic fish were gifts from Yingbing Zhong and Chunxin Fan (China Zebrafish Resource Center), respectively.

### Tissue Processing, Histology, and Immunohistochemistry

Histology, immunohistochemical staining, and RNA in situ hybridization were performed as described (Supporting Information Table S11) [7, 13]. The antibody specificity was tested in a zebrafish embryonic fibroblast cell line, *pac2* (Supporting Information Fig. S1).

### Morpholino Injections

Morpholinos were injected into the yolk sacs of embryos at the one-cell stage, as described [14]. Procedures for morpholino tissue injection were performed as described previously [7] with the following modifications. After amputation, morpholino was injected into the wound at three injection sites (1  $\mu$ l of 1 mmol each site) and electroporated four pulses at 50 V for 30 milliseconds with 5-second intervals using a BTX Electro Square Porator ECM 830 (BTX, San Diego, CA, <http://www.harvardapparatus.com/>). All morpholino oligonucleotides (Mo) were purchased from Gene Tools, LLC (Philomath, OR, <http://www.gene-tools.com/>). According to the manufacturer's recommendations, *Vivo-Morpholino* antisense oligonucleotides corresponding to zebrafish sequences of *foxi1*, *sox9a*, and *hoxa2b* mRNAs were directed against the translation start sites. A nonsense standard control morpholino was used to evaluate unspecific effects due to the morpholino injection. The morpholino efficiency was evaluated at protein level by quantitative comparison of immunohistochemical staining (Supporting Information Fig. S2) [13].

### RNA Deep Sequencing Analyses

Two intervals of Illumina RNA-deep sequencing were performed as described [7]. All data are available at the NCBI short read archive under study number SRA048162.1. All sequenced raw FASTQ data were mapped on the zebrafish reference genome (UCSC, danRer7) using Tophat. For each sample, we used Cuf-

flink [15] to analyze gene and transcript expressions. After the normalization of RNA read counts based on the library size, sequencing depth differences, and gene length differences, we conducted differential analysis for each pair of comparison groups using Cuffdiff software [15]. The differential expression (cut-off value) between two transcripts was defined as greater than twofold ( $\log_2$  ratio  $>1$ ) with  $p < .05$ .

### Functional Annotations

All differentially expressed gene and isoform sequences ( $q < 0.05$ ) were annotated in the gene ontology (GO) database ([www.geneontology.org](http://www.geneontology.org)) and the Kyoto Encyclopedia of Genes and Genomes (KEGG) pathway database ([www.genome.jp/kegg/pathway.html](http://www.genome.jp/kegg/pathway.html)). To compare two time points of samples with two replicates, we used R package (*goseq*) from bioconductor (<http://www.bioconductor.org/>) to implement enrichment analysis for GO annotation and pathways. The  $p$  values of the enrichment were calculated and adjusted to  $q$ -values for multiple testing corrections based on the hypergeometric distribution [16]. Meanwhile, the false discovery rate was determined according to Benjamini methods [17]. The generated database (time point-based differential GO analysis) was used for the hierarchical GO term network that we describe in the next section.

### Hierarchical GO Term Network

To generate the GO term network, we first identified all the superfamilies in superfamily (dcGO) and created files for them (BP\_SuperFam\_GO.txt, MF\_SuperFam\_GO.txt, and CC\_SuperFam\_GO.txt). The root of the category starts from this dcGO (<http://supfam.org/SUPERFAMILY/cgi-bin/dcgo.cgi>). Then, we downloaded the GO database and mounted it on Oracle. Based on the superfamilies, a script was written to retrieve the GO hierarchy down to the next level (GO\_Hier\_Tree.txt). Then, a program (PerlScript) was built to locate every daughter GO term. In order to avoid a recursive loop, we simply checked each of the parent GO ids and prevented them from appearing in the list of target daughter GO terms. Finally, we used the road map GO\_Hier\_Tree.txt (A file) to annotate the files of temporally differential GO analysis.

### Functional Classification and Clustering Enrichment

In order to understand the biological functions of unigene and isoforms, including the cluster of orthologous groups, we used the DAVID annotation system (<http://david.abcc.ncifcrf.gov/>) to perform functional classification and term enrichment [18, 19].

### Hierarchical Clustering of Differential Expression Data

To determine the similarity of differentially expressed genes between two time points, we performed hierarchical clustering. In hierarchical clustering, genes with similar expression patterns are grouped together and connected by a clustering tree or dendrogram. The distance in clusters among genes was calculated using SAS (SAS Institute, Inc., 2011, Cary, NC).

## RESULTS

### Wound Epidermis Constitution and Blastema Formation

Zebrafish epidermis consists of a surface layer, an intermediate layer, and a basal layer (Supporting Information Fig. S3).

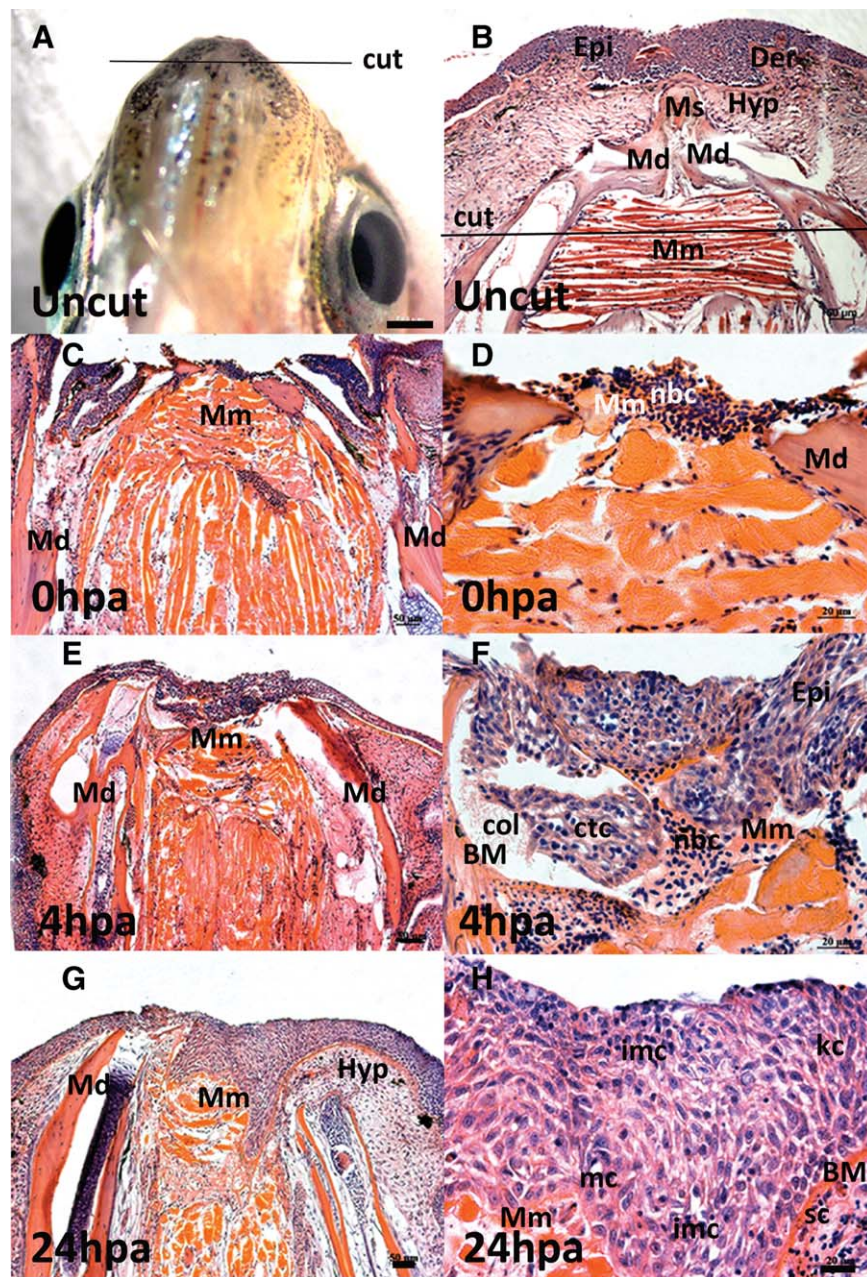


**Figure 1.** Re-epitheliation of the wound epidermis. Panels (A) and (B) show actual images of the intact lower jaw at the ventral side of the zebrafish head (A); and the histological structure of the intact lower jaw at transverse section and HE staining (B). The line demarcates the amputation plane in the following experiments. After amputation, blood cells (nbc) first accumulated on the wound muscle (Mm) (C, D), followed by epidermal cells and ctc from the surrounding tissues (E, F). These cells mixed with collagen matrix (col), reconstituted the wound epidermis, and underwent morphological changes toward epidermal cells. The cells with large, dark nuclei with little cytoplasm or having vacuolar cytoplasm are designated as the intermediate forms (imc) (G, H). HE staining; Scale bars (A) = 500  $\mu$ m; (B), (C), (E), (G) = 50  $\mu$ m; (D), (F), (H) = 20  $\mu$ m. Abbreviations: BM, basal membrane; ctc, connective tissue cells; Der, dermis; Epi, epidermis; Hyp, hypodermis; kc, keratine cells; mc, mucous cells; Md, mandible; Mm, mandibular muscle; Ms, mandibular symphysis; nbc, nucleated blood cells; sc, small nucleated cells.

Supposedly, the intermediate layer contains various types of differentiated and undifferentiated epidermal cells, while the basal layer is composed of undifferentiated cells and tightly links epidermis to dermis [20]. After a transverse removal of one-third of the mandible and associated epidermis, dermis, hypodermis, mandibular symphysis, and part of intermandibularis anterior (Fig. 1A, 1B), epidermis reconstitution was initiated following homeostasis. At least four sources of cells from

blood, epidermis, disrupted muscle, and associated connective tissues accumulated on the wound bed. These cells interweaved with collagen matrix and constituted wound epidermis (Fig. 1C–1F). At 24 hpa, the newly formed epithelium consisted of epidermal and intermediate cells (Fig. 1G, 1H). The intermediate cells displayed nuclear condensation and cytoplasmic shrinkage or vacuolation, and were morphologically between mesenchymal cells/nbc and epidermal

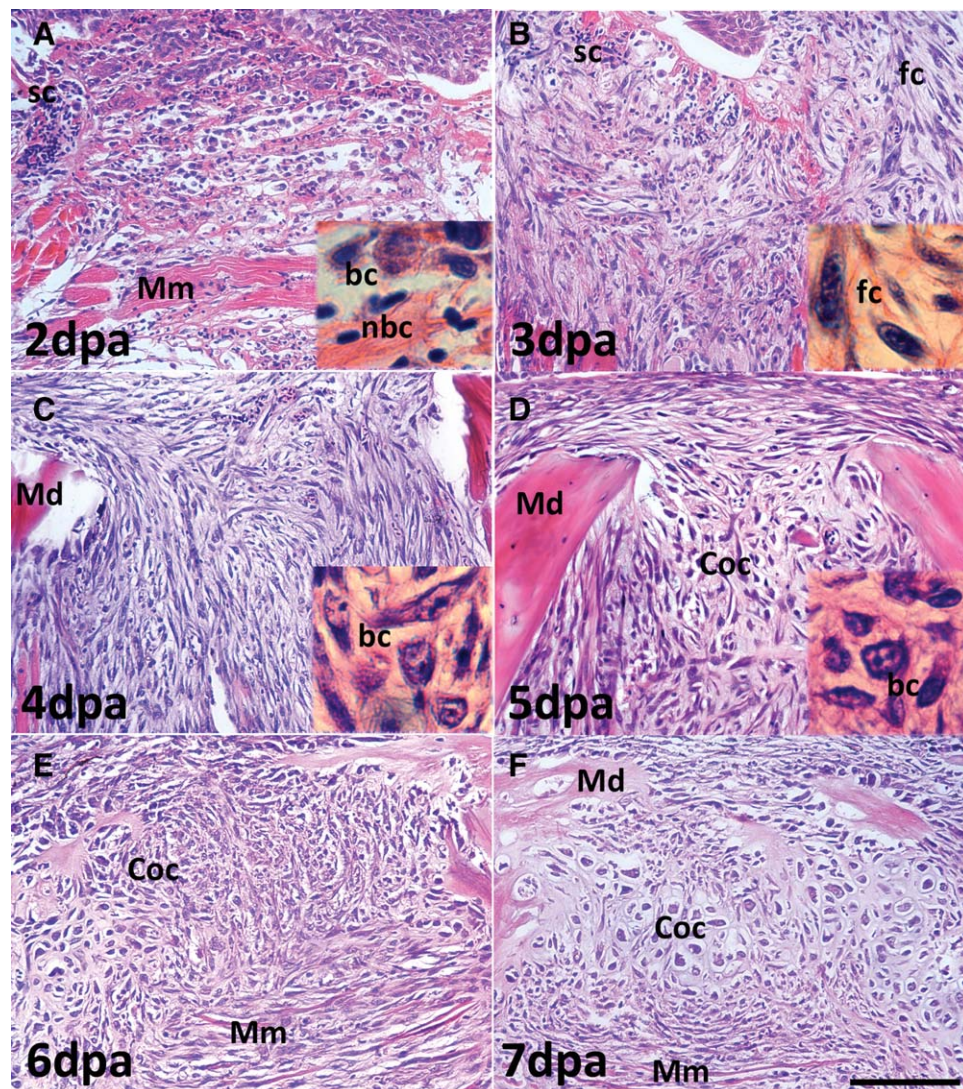


**Figure 2.** Cell type conversions in mesenchymal blastema and chondrogenic blastema from 2 dpa to 7 dpa. At 2 dpa, relatively undifferentiated bc were characterized by a high nucleus-to-cytoplasm ratio, clear nucleoli, and basophilic cytoplasm (A). With increased extracellular matrix, heterogeneous blastemal cells were activated, and became fc (B,C). Panels (D)–(F) show progressive differentiation and compartmentalization of blastemal cells toward Coc and Mm. Insets show the blastemal cell morphology by magnification of the same section. Scale bars = 100  $\mu$ m. Abbreviations: bc, blastemal cells; Coc, chondrogenic center; fc, fibroblast-like cells; Mm, mandibular muscle; sc, small nucleated cell.

keratinocytes/mucous cells. We attributed the complete re-epitheliation to cell-type conversions to tissue interactions between ectodermal-mesodermal components.

As the stratified epidermis covered the entire wound and tightly adhered to the wound's basal membrane, an aggregate of small nucleated cells (sc) with a minimal amount of cytoplasm emerged in the prospective blastema, just beneath the wound epidermis, at 1 dpa (Fig. 1H). When vasculogenesis and angiogenesis became active at 2 dpa, diverse cell types increased in number and gradually changed their morphology toward a fibroblast-like phenotype (Fig. 2A, 2B). On the fourth day, an expanding mesenchymal blastema was clearly visible, characterized by a mass of fibroblast-like blastemal cells (bc) packed in the increased extracellular matrix and fibrous tissues (Fig. 2C). On the fifth day, the blastemal cells in the central zone of the blastema were arranged circularly and converted into chondrogenic blastema. The cells located in

the outer area of the blastema became reorganized to resemble the shape and polarity of the adjacent tissues. Their long axes were oriented approximately parallel to the long axis of the adjoining mandible and muscle fiber (Fig. 2D–2F). We intended to determine which molecules mark the cell identity, and which signaling pathways orchestrate the dynamics of cell type conversion, angiogenesis, and extracellular matrix (ECM) deposition.

#### Deep Sequencing of Total RNAs from Four Significant Stages During Lower Jaw Regeneration

To obtain a comprehensive non-biased view of gene activity during different stages of jaw regeneration, we conducted a large scale deep sequencing of RNA samples. We monitored the changes in gene expression at four representative stages: uncut (0 hpa, hours postamputation), 2 hpa, 2 dpa (days post-amputation), and 5 dpa (Supporting Information Tables S1–

S4). Overall, 5,118 genes were significantly deregulated ( $q$ -value cut-off 0.05) in time between all four time points. Except for 67 genes that were regulated at all stages, wound healing and regeneration temporally altered the expression of 2,800 genes between 2 hpa and 0 hpa, 533 genes between 2 dpa and 2 hpa, and 240 genes between 5 dpa and 2 dpa (Supporting Information Fig. S4). This decreasing number of deregulated genes nicely paralleled the healing progress of lower jaw regeneration.

To evaluate the effectiveness of our GO-based annotations and differential analyses, we compared our readouts of extracellular matrix and chondrogenic signature gene clusters with the data from previous investigations [21, 22]. We found that the expressions of 50 out of 86 genes that are associated with ECM, chondrogenesis, and skeletal development, and 63% of development-associated genes (22/35) were altered (Supporting Information Table S5).

We then mapped the differentially expressed genes ( $p < .05$ ) to canonical pathways referred from the KEGG [23]. We compared this map with 10 major intracellular signaling pathways previously reported to be key players in initiating and maintaining the regeneration: MAPK, ErbB, Wnt, Notch, Hedgehog, TGF-beta, VEGF, ECM-receptor interaction, cell adhesion molecules, and Jak-STAT signaling pathways [24]. All these pathways were successfully identified in our time-lapse transcriptomal sequences of lower jaw regeneration.

Previous studies identified 21 genes during intestinal and body wall regeneration of *Apostichopus japonicus* [24]. In contrast, our study identified 281 candidate genes from the 1,191 genes that are associated with the 10 pathways (Supporting Information Table S6), accounting for 23.6% of total signaling steps. However, statistical analysis revealed that only 4 of the 10 pathways were significantly enriched (Supporting Information Table S7), suggesting distinct regenerative mechanisms responsible for lower jaw regeneration. Together, our temporal RNA-sequencing and GO term-annotation successfully identified the appropriate number of the deregulated genes, and thereby strengthened our ground work to further identify key signaling cascades responsible for lower jaw regeneration.

### Genome-Wide Annotation of Differential Transcripts to GO Term Networks

We annotated the differential transcripts and generated a tree diagram displaying all possible GO terms in networks. GO terms are organized hierarchically such that higher level terms are more general and thus are assigned to more genes, while descendant terms are more specific and related to parents.

We then identified the accumulation of protein identifiers assigned to a given GO term, and compared the ratio of proteins annotated to a given GO term to the total number of proteins available from the GO database. As an unbiased standard, we limited our GO term search to the top 3% of highly enriched terms and organized the accumulations according to the regenerative process (Supporting Information Table S8). Relative to preamputation (0 hpa), 28 GO terms were specifically accumulated at 2 hpa. These GO terms were highlighted in acute responses to the damage (Fig. 3A).

When comparing 2 dpa with 2 hpa, four temporally enriched terms were related to DNA replication: initiation, regulation of angiogenesis, heparin binding, and notochord cell differentiation. Eight terms were enriched at both 2 hpa

and 2 dpa, and were involved in epidermis development, angiogenesis, response to stimuli, and protein kinase/phosphatase activity. Until 5 dpa, significantly enriched genes were restricted to the sarcoglycan complex, and myosin filaments. Muscle fiber development was enriched at 2 dpa and 5 dpa (Fig. 3A).

### Functional Classification of Highly Enriched GO Term Subnodes

In this part of our study, we used DAVID Functional Annotation Clustering [18] to select common genes by examining annotations and identifying significantly shared GO terms. We also used the functional classification tool to quickly organize large lists of genes into functionally related groups. At 2 hpa, 244 upregulated ribonucleotide binding proteins were accumulated. This included 44 small GTP-binding proteins and 75 protein kinases. At 0 hpa, 29 genes that function in intracellular protein transport or cellular macromolecule localization were identified (Supporting Information Table S9).

When 2 dpa was compared with 2 hpa, 302 genes were upregulated, while 1,705 genes were downregulated ( $p < .05$ ). We detected a clear difference in upregulated proteins for the following GO terms: calcium ion binding, DNA replication, nucleosome assembly, and intermediate filament cytoskeleton. The 1,705 downregulated genes were significantly enriched in transmembrane, transporter activity, and transcription regulator activity. At 5 dpa, 410 genes were upregulated and 50 were downregulated. The 35 most accumulated genes were multiple Hox-, Fox-, and Sox-paralogs (Supporting Information Table S9).

GO classification and enrichment not only confirmed the GO terms associated with RNA processing, transcription regulation, GTP binding-protein kinase, transmembrane transporters, and calcium ion binding, but also functionally assigned the clustered genes to the superfamily level. We found that 10 superfamilies of Fox, Sox, Pax, POU, Six, Hox, Wnt, Bmp, Fgf, and Collagen enriched 101 deregulated genes (Fig. 3B). Thus, integration of functional classification into hierarchical GO trees permitted us to focus more on the GOs relevant to oxygen metabolism, angiogenesis, transmembrane transporters, GTPase-tyrosine kinase activity, DNA replication, neural crest cell migration, cell differentiation, axon extension, and epidermal and muscle development.

### Prediction of Signaling Cascades Associated with Regeneration Processes

To capture the difference in gene expression patterns and novel signaling pathways, we applied Euclidean distance measurement and performed a similarity search for common expression patterns of the target genes. Taking advantage of our identified GO-gene superfamily architecture (Fig. 3), we arbitrarily determined several index genes associated with the important GO terms and regenerative phenotypes, selected the top 30 of the most similarly changed genes (Supporting Information Table S10), and made predictions about the novel signaling connections.

To characterize the molecular mechanism of cell type conversions, we performed cluster analysis of two well-known marker genes associated with pluripotency: *pou5f1* and *foxo1b*. Among the genes differentially expressed between 2 hpa and 0 hpa, the top 30 genes with similar expression

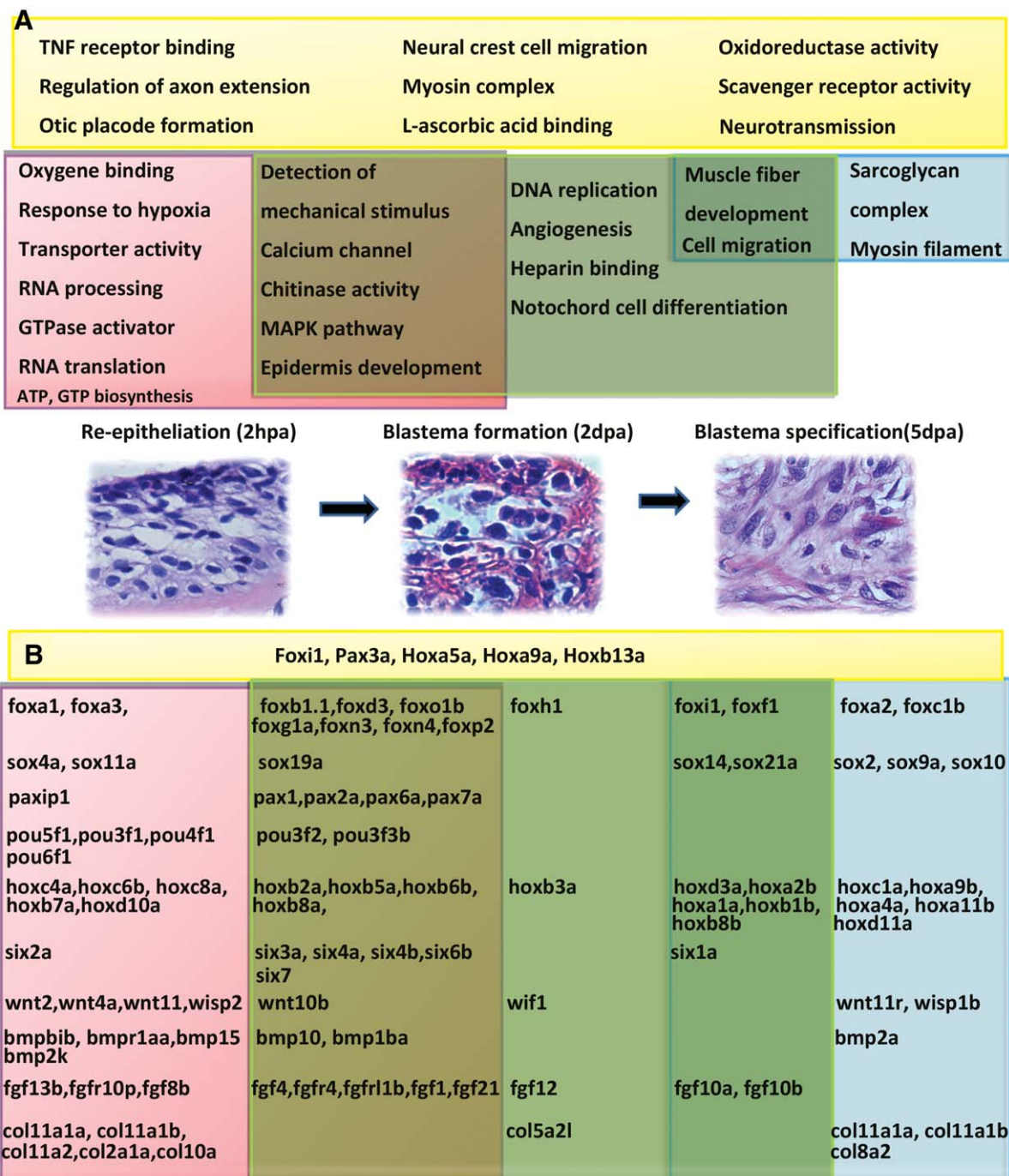


**Figure 3.** Integrative analyses of time point-based transcriptome establishes a gene ontology (GO) network and gene superfamily architecture. **(A):** Hierarchical GO-analysis reveals accumulation and connection of time point-based GO terms. The upper plate (yellow) shows the genes enriched at all time points. The middle plate shows the specific terms for each time point of the regenerative process. Each time point was indicated by a color (2 hpa in pink, 2 dpa in green, and 5 dpa in blue). The overlapping area shows the enriched genes linking the successive time points. Accumulation of time point-based connecting GO terms parallel to the successive cell type conversions from re-epitheliation to blastema formation to blastema specification (bottom plate). Panel **(B)** shows the enriched GO terms and 10 gene superfamilies by integration of hierarchy analysis into David functional classification. These deregulated genes contain inductive signals, blastemal border specifiers, tissue-specific specifiers, and pattern genes.

changes in the *pou5f1* cluster highly overlapped with the *cdx4*. *Cdx4-Hoxa9* and *Cdx4-Sall4* regulatory modules have been reported to respecify the hematopoietic and hemangioblast population [25, 26], while gene *kdrl*, also called *flk1*, is expressed in hemangioblasts. *kdrl* enhancer contains *cdx*-binding sites [27]. So, we examined these genes and found

that *cdx4*, *sall4*, *hox9a/b*, *hif1*, and *kdrl* were coincidentally activated at the early stage of jaw regeneration (Supporting Information Tables S1 and S2). In addition, activation of *hif1*, a master regulator of the hypoxia response and angiogenesis initiation (Supporting Information Table S10) [28], the *pou5f1-cdx4-kdrl* regulatory module was proposed to play a role in

blastemal angiogenesis and vasculogenesis. *foxo1b* shared a cluster with *pou3f1*, *foxi1*, *fhit*, and *enpp1* at 2 hpa. *pou3f1*, also known as *Oct-6*, is abundantly expressed in the epidermis and regulates epidermal cell differentiation [29]. Likewise, *foxi1* is recognized as an epidermal cell specification marker [30]. Since *enpp1*, a member of the ecto-nucleotide pyrophosphatase/phosphodiesterase family, influences a wide range of tissues through various signaling pathways [31], it is reasonable to converge *foxi1-foxo1b-pou3f1* signaling transduction with wound epidermis reconstruction.

Consistent with its function of global chromatin modification [32], *foxi1* was reactivated and formed a broadly mixed signal circuit at 5 dpa, including *bhlha15*, *sox10*, *tjp2a*, and *myod1* (Supporting Information Table S10). More broadly, the *foxi1-sox10-myod1* cluster interconnected with the *hoxa2b* and *pax3a* clusters. This *foxi1-hoxa2b-pax3a* broad signal circuit contained two *sox* (*sox21a*), three *fox* (*foxa2*, *foxf1*), and seven *hox* genes.

A myoprogenitor marker, *pax3a*, closely clustered with *matn3a*, which is usually present in the cartilage extracellular matrix. We found that *coll1a1a*, *coll1a2*, *annexin A6*, and *tgfb1* clustered together. The gene *tgfb1* encodes an ECM protein, and is reportedly involved in endochondrial bone formation in cartilage muscle fiber growth [33]. Coactivation of *coll1a1a*, *col112a*, *col2a1a*, and *pax3a* at 2 hpa and 5 dpa supported *pax3a-mant3a* association with cartilage collagens in the wound epidermis and chondrogenic blastema.

*Isl1* expression marks the multipotent stem cells, giving rise to a broad range of cardiovascular tissues, pharyngeal muscle, and the neural crest [34, 35]. *Isl1* is also required for multiple aspects of motor neuron development [36]. At the initial phase of jaw regeneration, *isl1* was upregulated with *wnt11*, *fgf8b*, and *cdh7*, genes which have kinase and GTPase activity, the ATP-binding cassette, and structural elements of the cytoskeleton, such as *riok2*, *sgk2a*, and *abcf2*. Unexpectedly, *sox9a* clustered with the genes annotating the planar cell polarity (PCP) signaling components (*fzd7a*, *prickle1*) at 5 dpa. It is likely that *wnt11* and *fgf8b* act as directional cues to regulate the PCP pathway and small GTPase signaling in *isl1*-positive and *sox9a*-positive cells during wound epidermis and chondrogenic blastema reorganization. Altogether, we identified four signal pathways orchestrating lower jaw regeneration. As shown in Supporting Information Table S10, these pathways are directly or indirectly linked to Rho-GTPase and MAPK pathways.

### Wound Epidermis and Blastema Display Characteristic Expression Patterns

To test our proposed signaling pathways and evaluate the utility of transcript profiling for prediction of protein expression levels, we examined the cellular expression patterns of selected several index genes. In the uncut lower jaw, Foxi1 protein was localized primarily in the epidermis and sparsely in the dermis (Figs. 4A, 5A), whereas Pax3a was mainly distributed in connective tissues (Fig. 4C). Sox9a and Sox9b were differentially and weakly expressed in the mandible periosteum and muscle (Fig. 4F, 4G). After amputation, Foxi1 was rapidly induced in wound epidermis and the surrounding normal epidermis as well as in the presumptive blastema of small nucleated cells and fragmented muscle cells (Figs. 4B, 5B, 5C). In comparison with the even induction of Sox9b in the wound

epidermis (Fig. 4G, 4H), wounding strongly induced Pax3a expression in the basal layer (Figs. 4C, 4D, 5G).

While Foxi1-expression increased at the surface of the wound epidermis and decreased in the presumptive blastema region (3 dpa), Hoxa2b and Pax3a expression increased and spread from the basal layer to the blastema (Fig. 5H, 5I, data not shown). At 7 dpa, Hoxa2b- and Pax3a-expressing mesenchymal blastema encompassed Sox9a-expressing chondrogenic blastema (Fig. 5J–5M). These observations suggested that epidermis reconstitution and blastema formation can be characterized by the regional and dynamic expression of Foxi1, Pax3a, Hoxa2b, and Sox9a/b.

Unlike Foxi1 expression in the surface layer of the epidermis, Mek1/2 was expressed in the epidermal basal layer, Meckel's surroundings, and intramuscular connective tissue. Like Foxi1, p-Erk1/2 was expressed in small nucleated cells and certain fragmented muscle cells in the newly forming hypodermis between the wound epidermis and muscle (Fig. 5D–5F). Temporospatial colocalization of Mek1/2 and p-Erk1/2 with Pax3a and Foxi1 during wound epidermis reconstitution and generation of blastema progenitors in the prospective mesenchymal blastema suggest that the expression of Foxi1 and Pax3a not only acts as an active cell identity marker, but also regulates cell fate through the MAPK and ERK pathways.

### Cellular Transformation and Tissue Compartments of Three Cell Lineages

To visualize blastema formation and cell identity conversions in the *in vivo* environment, we used three transgenic fishes with fluorescent labeling: *flk1:EGFP* [37], *pou5f1:EGFP* [12], and *isl1:GFP* [38]. These lines express GFP under the control of the tissue-specific promoter. The GFP expression patterns recapitulate the endogenous expression of the corresponding genes (Supporting Information Fig. S5).

In uncut fish, *flk1/kdr1:GFP* transgene (hereafter referred to as *flk1-GFP*) was expressed specifically in the blood vessels in the hypodermis and muscle (Fig. 6A). Angiogenic sprouting of blood vessels occurred in the wound muscle tissues as an initial response to amputation at 2 hpa. This response was followed by the emergence of GFP-expressing cells in the newly regenerating hypodermis (prospective blastema, Fig. 6B, 6C). Over the following 2 days, GFP-vasculature was transiently expressed and GFP-expressing cells increased. These cells constituted one-third of all blastema cells (Fig. 6D, 6E). At 5 dpa, only a few GFP-positive cells remained in the hypodermis and chondrogenic center (Fig. 6F). The sustainable and bright fluorescent signal in blastemal cells and intermittent fluorescence in the blastema vasculature was consistent with the previous report that Flk1 expression is stronger in developing angioblast/endothelial precursors than in mature vessels [39, 40].

Flk1-GFP positive blastemal cells were not contained by Foxi1, Sox9a, or Sox9b antibodies (Fig. 6F–6H), presumably representing Flk1-positive hemangioblasts. In *pou5f1*-promoter-driven GFP transgenic fish, GFP-positive cells were only harbored in the dermis-hypodermis adjacent to the Meckel's cartilage (Fig. 4F). After amputation, *pou5f1-GFP* signals were detected in the intermuscular vasculature within the presumptive blastema region at 14 hpa (Fig. 4H). Thus, the *pou5f1* gene was actively promoted in vascular cells. These observations suggest that wounding induced a double

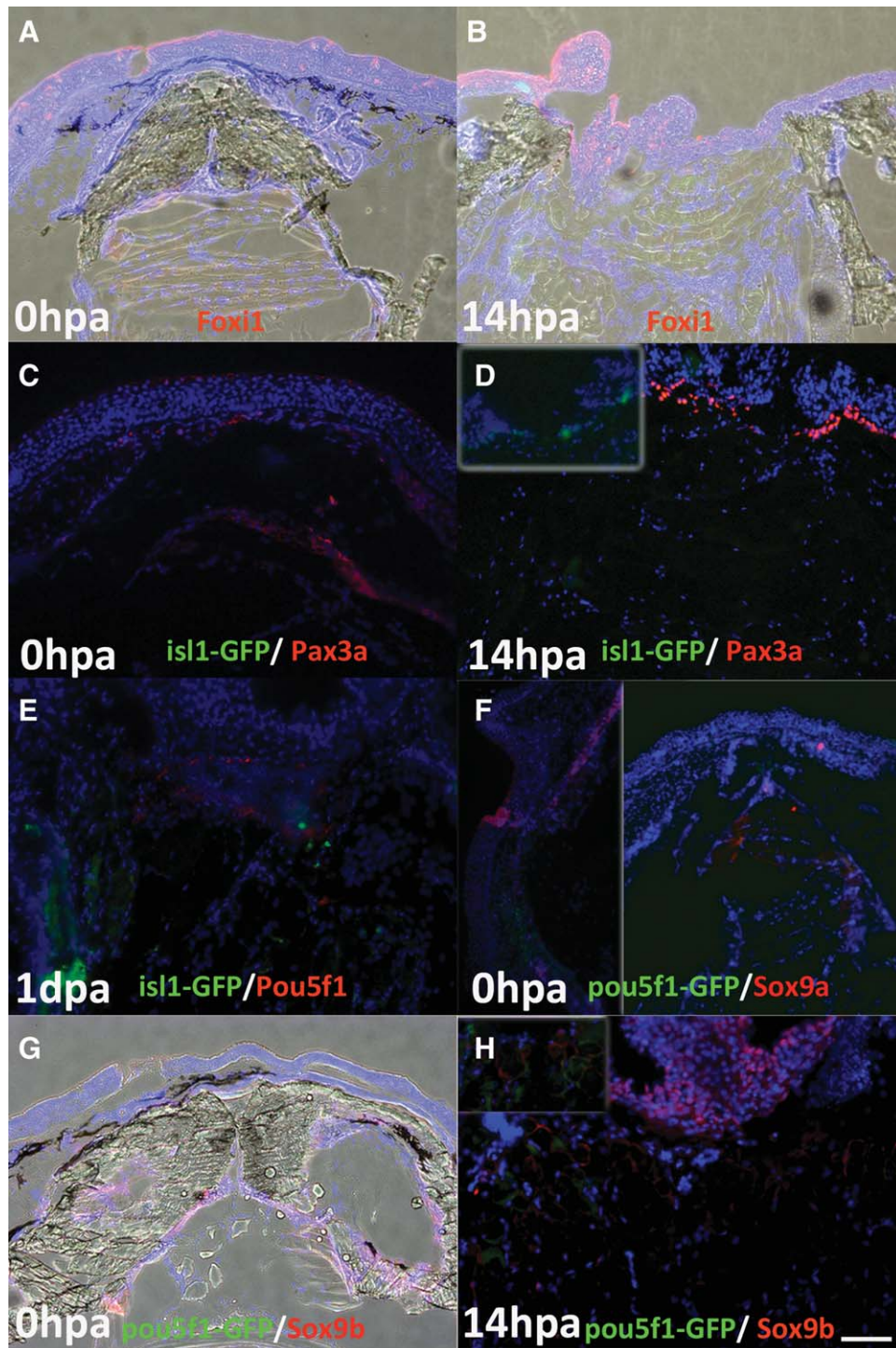


**Figure 4.** Initial induction of five index genes. Compared to preamputation (0 hpa), wounding induced an immediate increase of Foxi1 expression in the wound epidermis and on the surface of the surrounding normal epidermis at 14 hpa (**A**, **B**). In *Isl1*-GFP transgenic fish, wounding prompted quick induction of Pax3a in the basal layer of regenerating epidermis (**C**, **D**), *Isl1*-GFP in basal layer cells and intramuscular connective tissues like peripheral nerves (**C**–**E**), and Pou5f1 in the adjoining area between wound epidermis and wound muscle (**E**). The inset of (**D**) highlights *Isl1*-GFP positive cells along the basal layer. Panels (**F**)–(**H**) show weak expression of Sox9a, Sox9b, and *pou5f1*-GFP in *pou5f1*-GFP transgenic fish. Sox9b expression was significantly increased in the wound epidermis (**H**). Activation of *pou5f1*-GFP transgene is highlighted in (**H**) inset. Scale bars (**A**), (**B**), (**F**), (**G**) = 100 μm; (**C**), (**D**), (**E**), (**H**) = 50 μm. Abbreviation: GFP, green fluorescent protein.

process of blastemal angiogenesis and vasculogenesis, possibly by dedifferentiation of hemangioblast derivatives (Fig. 6A–6E).

*Isl1*-GFP has been reported to be expressed in the cranial motor and sensory neurons (Supporting Information Fig. S2) [38]. Here, we found that wounding induced *Isl1*-driven GFP

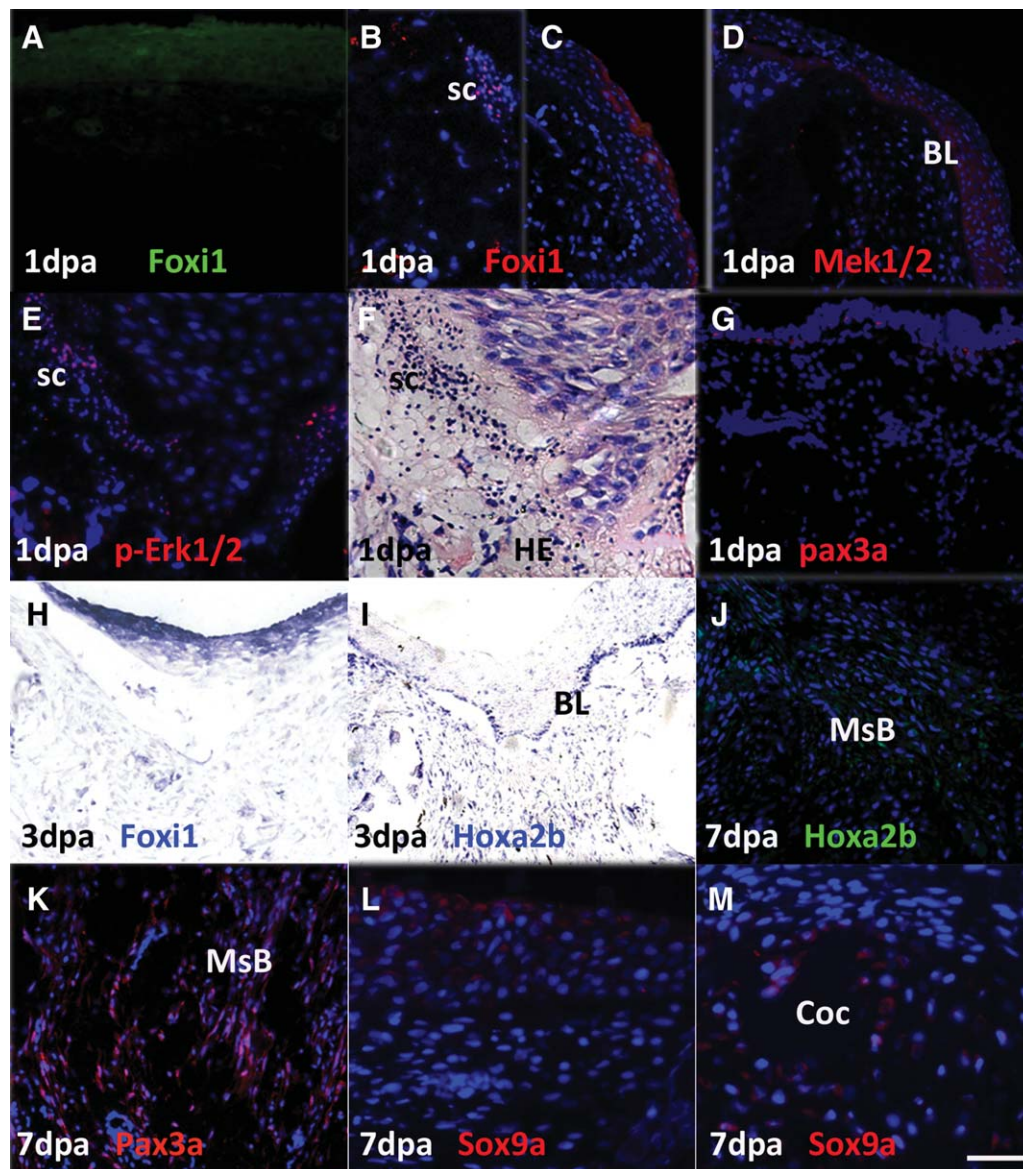


**Figure 5.** Dynamic expression profile of several regeneration-related genes. Foxi1 was expressed in normal epidermis and hypodermis (A). After amputation, Foxi1 expression increased in the surrounding normal epidermis. Wounding also induced Foxi1 and P-Erk1/2 expression in small nucleated cells (sc) and damaged muscles (B, C, E). With an increase on the epidermal surface at 3 dpa, Foxi1 decreased in the blastema region (H). Mek1/2, Hoxa2b, and Pax3a were initially induced in epidermal basal cells (D, G, I), and then increased in the mesenchymal blastema (J, K). During blastema respecification, Sox9a was induced in epidermis and chondrogenic blastema (L, M). Panel (F) shows H&E staining of (E). Panels (H) and (I) show antibody-alkaline phosphatase-NBT staining. The remaining figures were stained with fluorescence-conjugate secondary antibodies. Blue indicates DAPI staining. Scale bars (B), (E), (L), (M) = 25  $\mu$ m; the rest = 50  $\mu$ m. Abbreviations: BL, basal layer of wound epidermis; Coc, chondrogenic center; fmc, fragmented muscle; Mc, Meckel's cartilage; md, mandible; MsB, mesenchymal blastema; sc, small nucleated cells.

expression in the new regenerating basal layer of wound epidermis and blastemal region (Fig. 4C–4E). Initially, a stream of *Isl1*-GFP expression extended along the basal layer of the wound regenerating epidermis, partially overlapping with Pax3a (Fig. 4D). At 1 dpa, *Isl1*-GFP largely appeared at Meckel's cartilage and dotted at the presumptive blastema region (Fig. 4E). At 6 dpa, *Isl1*-GFP-expression remained at the chondrogenic centers (Coc) (Fig. 6I). We found that *Isl1*-GFP partially overlapped with the immunostaining of axonemal  $\alpha$ -tubulin. In contrast to more tubulin staining in the intermandibularis posterior area, more *Isl1*-GFP expressing cells were observed in the intermandibularis anterior region (Supporting

Information Fig. S6). These findings suggest that activation of *Isl1* signaling may represent dedifferentiation of neuro-neural crest derivatives and extension of injured nerve fibers.

#### Foxi1 Is Required to Modulate Epidermis Reconstitution and Blastema Formation

We have reported that Foxi1 is required for proper growth of the lower jaw during embryonic development and adult regeneration [7, 14]. Now, we note that Foxi1 proteins are mostly distributed in the epidermis, with some in the blastema. In the Morpholino-control animals, wounding induced Foxo1b and Pax3a expression, largely in the basement of the

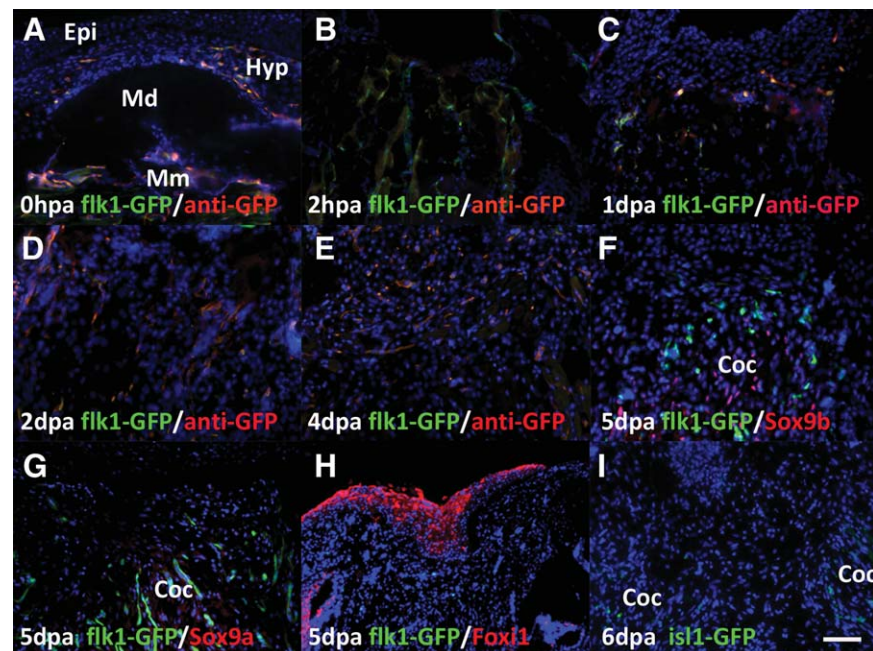


**Figure 6.** Visualization of expression of flk1-GFP and isl1-GFP transgenes during blastema regeneration. In flk1-GFP transgenic fish, flk1-expressing cells first occurred in the newly formed hypodermis, and then spread to the vessel-rich muscle; the expression pattern of flk1-GFP mirrored that of 594-daylight-conjugate anti-GFP in immunohistochemistry (A–F). During blastema chondrogenic respecifications (5 dpa, 6 dpa), flk1-GFP, isl1-GFP, Sox9a-, Sox9b-, and Foxi1-expressing cells only remained in the Coc. Obviously, flk1-GFP (green) did not costain with antibodies Sox9b, Sox9a, or Foxi1 (F–I). Scale bars = 50  $\mu$ m. Abbreviations: Coc, chondrogenic center; GFP, green fluorescent protein.

regenerating epidermis at 1 dpa. Foxi1-Morpholinos caused expansion of Foxo1b- and Pax3a-expressing cells into the damaged muscle (Supporting Information Fig. S7A–S7D). Perturbation of Foxi1 signaling also impaired blastema vasculogenesis, without affecting flk1-GFP expression in the surrounding muscle (Supporting Information Fig. S7E, S7F). These results suggest that Foxi1 not only promotes specification of epidermal ectoderm but also inhibits blastema formation.

#### Foxi1, hoxa2b, and sox9a Crossregulate to Reciprocally Maintain Expression Patterns

To trace back to the embryonic compartments of Foxi1-expressing cells, we examined the embryonic expression patterns of *foxi1*, *hoxa2b*, and *sox9a/b* by combining RNA knock-down techniques with whole mount RNA in situ hybridization (Fig. 7). In agreement with the previous reports, we found that all four genes are expressed on the midbrain and/or hindbrain and pharyngeal arches during embryonic jaw development (48–55 hpf) [14, 41, 42]. Microinjection of antisense *sox9a*-Mo caused a reduction of both *foxi1* (Fig. 7A, 7B) and *hoxa2b* domains (Fig. 7D, 7E) in the pharyngeal arches, while their expression in the mid-hind brain was not altered. *hoxa2b* morphants displayed an expansion of *sox9a* domain in myelencephalon (Fig. 7G, 7H) and a slight diffusion of *foxi1* (Fig. 7A, 7C). In the *foxi1*-Mo embryos, however, the expressing domains of both *hoxa2b* (Fig. 7D, 7F) and *sox9a* (Fig. 7G, 7I) were strikingly expanded in the branchial arches, and showed a Mo-foxi1 concentration-dependent effect (Supporting Information Fig. S8). In accordance with Foxi1 protein's inhibitory effects on Foxo1b<sup>+</sup> and Pax3a<sup>+</sup> cell expansion, *foxi1* transcript represses expansion of *hoxa2b*- and *sox9a*-

transcription domains. These results suggested that specification of *sox9a*- and *hoxa2b*-expressing cells to the pharyngeal arch components requires a downregulation of *foxi1*.

#### DISCUSSION

Regenerative medicine offers hope to patients by replacing damaged tissues with readily available sources. The most attractive strategy is to convert the available cells into the desired cell types [43]. To fulfill this promise, recent efforts have focused on the development of biomaterials to aid in the healing response and/or to provide a scaffold that can promote appropriate tissue formation [44]. We have shown that zebrafish amputation can induce successive cellular transformation and create two transitional blastemal structures/mesenchymal and chondrogenic blastema. In this study, we could not clearly identify which biomaterials would trigger successive cell-based regeneration after lower jaw injury. However, our integrative RNA-sequencing analyses identified four novel signaling pathways which orchestrate the progressive cell-type conversions and tissue reorganization. We propose the following model for blastema regeneration of the lower jaw.

1. Foxi1 and Pax3a signaling axes coordinately orchestrate wound epidermis reconstruction and blastema formation. During lower jaw regeneration, an initial response (0–24 hpa) to wound signaling is collagen deposition, corresponding with upregulation of *col11a1a*, *col11a2*, and *col2a1a* genes. These activities include Foxi1-expression on the surface layer of the epidermis, Pax3a- and Hoxa2b-expression in the basal layer of epidermis, and Sox9b-expression on the whole epidermis. Various types of cells accumulate

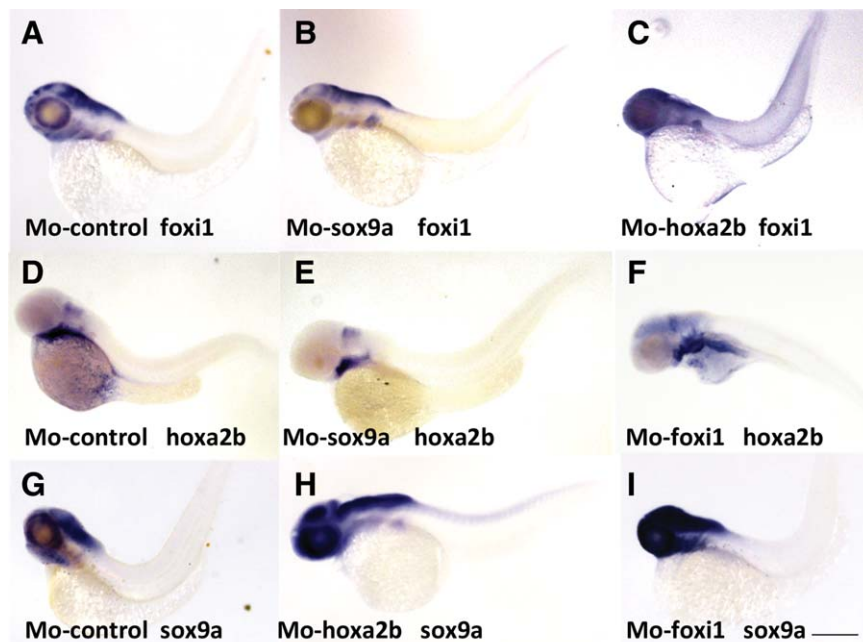


**Figure 7.** Analyses of *foxi1*, *sox9a*, and *hoxa2b* expression by whole mount embryo in situ hybridization combined with morpholino injection. The standard control morpholino (A, D, G), or the gene-specific morpholino of either *foxi1*-Mo (F, I), *hoxa2b*-Mo (C, H), or *sox9a*-Mo (B, E) was separately microinjected into embryos 48–55 hpf (hour postfertilization). Compared with microinjection of standard control morpholino, the changes of expression patterns are shown in (A–C) for *foxi1*; in (D–F) for *hoxa2b*; and (G–I) for *sox9a*. Although *sox9b* is also expressed in mid-hind brain and pharyngeal arches, its expression is scarcely altered by *foxi1*-Mo, *hoxa2b*-Mo, or *sox9a*-Mo (data not shown). Each microinjection contains 1  $\mu$ l of 0.1 mM morpholino. Scale bars = 250  $\mu$ m.

along the deposited collagen matrix. The regional and dynamic expression of *Foxi1*, *Pax3a*, *Hoxa2b*, *Sox9a/b*, *Pou5f1*, and *Isl1* indicates that *Pax3a*<sup>+</sup> basal layer cells arise from the interactions between immigrated epidermal cells and the wound mesodermal tissues, and subsequently differentiate into *Foxi1*<sup>+</sup>/*Sox9b*<sup>+</sup> epidermal cells or *Hoxa2b*<sup>+</sup>/*Pax3a*<sup>+</sup> blastemal cells. The multipotent characteristic of regenerating basal layer cells resembles the regenerative capability of EPI-NCSC [45].

How do *Pax3a*-expressing mesenchymal cells become multipotent epidermal cells? In mice, *pax3* activation promotes the differentiation of mesenchymal stem cells toward the myogenic lineage and regulates mesenchymal-epithelial interconversion [46–48]. In zebrafish mandible regeneration, we propose that the *pax3a*-*mant3a*-cartilage collagen pathway designs cell-type conversions. Different from skin development in which *col1a2* transcript is strongly expressed in the basal layer of epidermal and dermal endothelial cells [49], expression of cartilaginous collagen type XI and type II in regenerating tissues can provide structural support, and orientation for epidermal cells and blastemal cells.

A related question is why blastema formation proceeds from re-epitheliation. Zebrafish epidermis contains diverse cell types, including a variety of subtypes of ionocytes. *Foxi1* regulates H<sup>+</sup>-ATPase-rich cell differentiation [20]. From thousands of deregulated genes, we identified *foxi1-foxo1b-pou3f1* cluster signals. This pathway may promote differentiation of *Pax3a*<sup>+</sup> progenitors into *Foxi1*-expressing epidermal cells. In the blastema, *Foxi1* represses expansion of *hoxa2b/pax3a*, and favors mesenchymal-chondrogenic blastema transition. This signal switch can explain how *Foxi1* alternatively promotes re-epitheliation before blastema respecification.

2. *pou5f1-cdx4-kdrl* signaling pathway regulates blastemal angiogenesis and vasculogenesis.

Most published studies suggest that blastema formation follows a process of dedifferentiation of mesodermal tissues

and cells derived from the neural crest [50, 51]. Our cell morphology and differentiation analyses have indicated that multiple cell sources, including blood-derivative cells, are dedifferentiated into blastemal progenitors [7]. In this study, we supplemented blastema formation with *Pax3a*-mediated cell type conversions. Additionally, pluripotent-associated factor *pou5f1* grouped with hematopoietic activator *cdx4* and endothelium-specific receptor tyrosine kinase *kdrl* gene. This pathway is supposed to regulate hemangioblast-derived blastemal angiogenesis and vasculogenesis.

3. Neuronal PCP signaling pathways regulate positional patterning in blastema regeneration.

It has been reported that the positional identity of the blastema correlates with the characteristic expression pattern of Hox genes [7] and *FoxD* [52]. Now, we find that *wnt11*-PCP pathways are induced during re-epitheliation and chondrogenic blastema respecifications. In the initial phase, the *wnt11*-PCP pathway components direct asymmetric distribution of *isl1* signaling in the injured cranial nerves and muscles (Supporting Information Fig. S5). During blastema respecification (5 dpa), the *wnt11r*-PCP pathway links to *sox9a* in blastema transient chondrogenesis. Given that core PCP genes are crucial for the development and function of the nervous system and are involved in neural tube closure, ependymal polarity, neuronal migration, and axon guidance [53, 54], the *Isl1*-*wnt11*-PCP-*sox9a* pathways could provide instructions for the cartilage matrix in tissue patterning and polarize the motile behaviors of blastemal cells with respect to the anteroposterior axis.

## CONCLUSIONS

According to the dynamic signaling changes and successive cellular transformation during regeneration of zebrafish lower jaws, we propose a jaw-regeneration gene network that converges the *pouf51-cdx4-kdrl*, *pax3a-mant3a-col11*, *isl1-wnt11*-

*PCP-sox9a*, *foxi1-foxo1b-pou3f1* signaling axes onto small GTPase-MAPK pathways to define wound epidermis reconstruction, blastema formation, and blastemal cell lineage specification. Further studies of these pathways will identify the crucial molecular drivers involved and potential therapeutic targets. This study therefore provides a signaling roadmap to study vascular tissue engineering and skin stem cell-based regenerative therapy.

#### ACKNOWLEDGMENTS

We thank Kathy Kyler for editing the manuscript. We appreciate Wei Zhen, Ying Zhang, Qin Yang, Junhui Cao, and Xiaoyun Zhou for their technical assistance. We are indebted to Guan-jie Chen and Suiyuan Zhang for their valuable computational analysis in RNA deep sequencing. This work was supported in part by the Innovation Program of Shanghai Municipal Education Commission (13ZZ126) to J.Y., the International Cooper-

ation Initiative Program of Shanghai Ocean University (A2302110002) to J.Y., and Shanghai Universities First-class Disciplines Project of Fisheries.

#### AUTHOR CONTRIBUTIONS

J.Y.: conception and design, financial support, data analysis and interpretation, and manuscript writing; H.Z., X.W., K.L., and S.G.: collection and/or assembly of data and data analysis and interpretation; C.F.: provision of study material; G.W.: RNA-seq data analysis; X.Z.: manuscript writing. H.Z., X.W., and K.L. are joint first authors.

#### DISCLOSURE OF POTENTIAL CONFLICTS OF INTEREST

The authors indicate no potential conflicts of interest.

#### REFERENCES

- Poss KD. Advances in understanding tissue regenerative capacity and mechanisms in animals. *Nat Rev Genet* 2010;11:710–722.
- Whited JL, Tabin CJ. Regeneration review reprise. *J Biol* 2010;9:15.
- Fisher MB, Mauck RL. Tissue engineering and regenerative medicine: Recent innovations and the transition to translation. *Tissue Eng Part B Rev* 2013;19:1–13.
- Nemeno-Guanzon JG, Lee S, Berg JR et al. Trends in tissue engineering for blood vessels. *J Biomed Biotechnol* 2012;2012:956345.
- Nowak JA, Polak L, Pasolli HA et al. Hair follicle stem cells are specified and function in early skin morphogenesis. *Cell Stem Cell* 2008;3:33–43.
- Tasoglu S, Demirci U. Bioprinting for stem cell research. *Trends Biotechnol* 2013;31:10–19.
- Wang X, He H, Tang W et al. Two origins of blastemal progenitors define blastemal regeneration of zebrafish lower jaw. *PLoS One* 2012;7:e45380.
- Yannas IV. Emerging rules for inducing organ regeneration. *Biomaterials* 2013;34:321–330.
- Borchardt T, Looso M, Bruckskotten M et al. Analysis of newly established EST databases reveals similarities between heart regeneration in newt and fish. *BMC Genomics* 2010;11:4.
- Monaghan JR, Epp LG, Putta S et al. Microarray and cDNA sequence analysis of transcription during nerve-dependent limb regeneration. *BMC Biol* 2009;7:1.
- Qin YF, Fang HM, Tian QN et al. Transcriptome profiling and digital gene expression by deep-sequencing in normal/regenerative tissues of planarian *Dugesia japonica*. *Genomics* 2011;97:364–371.
- Parvin MS, Okuyama N, Inoue F et al. Autoregulatory loop and retinoic acid repression regulate *pou2/pou5f1* gene expression in the zebrafish embryonic brain. *Dev Dyn* 2008;237:1373–1388.
- Sun D, Zhang Y, Wang C et al. Sox9-related signaling controls zebrafish juvenile ovary-testis transformation. *Cell Death Dis* 2013;4:e930.
- Nissen RM, Yan J, Amsterdam A et al. Zebrafish *foxi* one modulates cellular responses to Fgf signaling required for the integrity of ear and jaw patterning. *Development* 2003;130:2543–2554.
- Trapnell C, Hendrickson DG, Sauvageau M et al. Differential analysis of gene regulation at transcript resolution with RNA-seq. *Nat Biotechnol* 2013;31:46–53.
- Young MD, Wakefield MJ, Smyth GK et al. Gene ontology analysis for RNA-seq: Accounting for selection bias. *Genome Biol* 2010;11:R14.
- Yekutieli DBY. Resampling-based false discovery rate controlling multiple test procedures for correlated test statistics. *J Stat Plan Inference* 1999;82 171–196.
- Huang da W, Sherman BT, Lempicki RA. Systematic and integrative analysis of large gene lists using DAVID bioinformatics resources. *Nat Protoc* 2009;4:44–57.
- Huang da W, Sherman BT, Zheng X et al. Extracting biological meaning from large gene lists with DAVID. *Curr Protoc Bioinformatics* 2009;Chapter 13:Unit 13 11.
- Chang WJ, Hwang PP. Development of zebrafish epidermis. *Birth Defects Res C Embryo Today* 2011;93:205–214.
- Andreasen EA, Mathew LK, Tanguay RL. Regenerative growth is impacted by TCDD: Gene expression analysis reveals extracellular matrix modulation. *Toxicol Sci* 2006;92:254–269.
- Herlofsen SR, Kuchler AM, Melvik JE et al. Chondrogenic differentiation of human bone marrow-derived mesenchymal stem cells in self-gelling alginate discs reveals novel chondrogenic signature gene clusters. *Tissue Eng Part A* 2011;17:1003–1013.
- Kanehisa M, Goto S, Kawashima S et al. The KEGG resource for deciphering the genome. *Nucleic Acids Res* 2004;32:D277–280.
- Sun L, Chen M, Yang H et al. Large scale gene expression profiling during intestine and body wall regeneration in the sea cucumber *Apostichopus japonicus*. *Comp Biochem Physiol Part D Genomics Proteomics* 2011;6:195–205.
- Davidson AJ, Ernst P, Wang Y et al. *cdx4* mutants fail to specify blood progenitors and can be rescued by multiple *hox* genes. *Nature* 2003;425:300–306.
- Yan J, Chen YX, Desmond A et al. *Cdx4* and *menin* co-regulate *Hoxa9* expression in hematopoietic cells. *PLoS One* 2006;1:e47.
- Ishitobi H, Wakamatsu A, Liu F et al. Molecular basis for *Flk1* expression in hemato-cardiovascular progenitors in the mouse. *Development* 2011;138:5357–5368.
- Dewhirst MW, Cao Y, Li CY et al. Exploring the role of HIF-1 in early angiogenesis and response to radiotherapy. *Radiother Oncol* 2007;83:249–255.
- Faus I, Hsu HJ, Fuchs E. Oct-6: A regulator of keratinocyte gene expression in stratified squamous epithelia. *Mol Cell Biol* 1994;14:3263–3275.
- Kwon HJ, Bhat N, Sweet EM et al. Identification of early requirements for preplacodal ectoderm and sensory organ development. *PLoS Genet* 2010;6:e1001133.
- Mackenzie NC, Huesa C, Rutsch F et al. New insights into NPP1 function: Lessons from clinical and animal studies. *Bone* 2012;51:961–968.
- Yan J, Xu L, Crawford G et al. The forkhead transcription factor *Foxl1* remains bound to condensed mitotic chromosomes and stably remodels chromatin structure. *Mol Cell Biol* 2006;26:155–168.
- Kim HR, Ingham PW. The extracellular matrix protein TGFBI promotes myofibril bundling and muscle fibre growth in the zebrafish embryo. *Dev Dyn* 2009;238:56–65.
- Bu L, Jiang X, Martin-Puig S et al. Human *ISL1* heart progenitors generate diverse multipotent cardiovascular cell lineages. *Nature* 2009;460:113–117.
- Harel I, Nathan E, Tirosh-Finkel L et al. Distinct origins and genetic programs of head muscle satellite cells. *Dev Cell* 2009;16:822–832.
- Liang X, Song MR, Xu Z et al. *Isl1* is required for multiple aspects of motor neuron development. *Mol Cell Neurosci* 2011;47:215–222.

- 37** Choi J, Dong L, Ahn J et al. FoxH1 negatively modulates flk1 gene expression and vascular formation in zebrafish. *Dev Biol* 2007;304:735–744.
- 38** Higashijima S, Hotta Y, Okamoto H. Visualization of cranial motor neurons in live transgenic zebrafish expressing green fluorescent protein under the control of the islet-1 promoter/enhancer. *J Neurosci* 2000;20:206–218.
- 39** Jin SW, Beis D, Mitchell T et al. Cellular and molecular analyses of vascular tube and lumen formation in zebrafish. *Development* 2005;132:5199–5209.
- 40** Liao W, Bisgrove BW, Sawyer H et al. The zebrafish gene *cloche* acts upstream of a flk-1 homologue to regulate endothelial cell differentiation. *Development* 1997;124:381–389.
- 41** Hunter MP, Prince VE. Zebrafish hox paralogue group 2 genes function redundantly as selector genes to pattern the second pharyngeal arch. *Dev Biol* 2002;247:367–389.
- 42** Yan YL, Willoughby J, Liu D et al. A pair of Sox: Distinct and overlapping functions of zebrafish *sox9* co-orthologs in craniofacial and pectoral fin development. *Development* 2005;132:1069–1083.
- 43** Cohen DE, Melton D. Turning straw into gold: Directing cell fate for regenerative medicine. *Nat Rev Genet* 2011;12:243–252.
- 44** Fisher MB, Mauck RL. Starting with form, emerging with function: Nanofibrous scaffolds for tissue engineering of orthopedic tissues. *Nanomedicine (Lond)* 2013;8:505–508.
- 45** Sieber-Blum M, Hu Y. Epidermal neural crest stem cells (EPI-NCSC) and pluripotency. *Stem Cell Rev* 2008;4:256–260.
- 46** Gang EJ, Bosnakovski D, Simsek T et al. Pax3 activation promotes the differentiation of mesenchymal stem cells toward the myogenic lineage. *Exp Cell Res* 2008;314:1721–1733.
- 47** Wiggan O, Fadel MP, Hamel PA. Pax3 induces cell aggregation and regulates phenotypic mesenchymal-epithelial interconversion. *J Cell Sci* 2002;115:517–529.
- 48** Wiggan O, Shaw AE, Bamberg JR. Essential requirement for Rho family GTPase signaling in Pax3 induced mesenchymal-epithelial transition. *Cell Signal* 2006;18:1501–1514.
- 49** Le Guellec D, Morvan-Dubois G, Sire JY. Skin development in bony fish with particular emphasis on collagen deposition in the dermis of the zebrafish (*Danio rerio*). *Int J Dev Biol* 2004;48:217–231.
- 50** Nakatani Y, Kawakami A, Kudo A. Cellular and molecular processes of regeneration, with special emphasis on fish fins. *Dev Growth Differ* 2007;49:145–154.
- 51** Satoh A, Graham GM, Bryant SV et al. Neurotrophic regulation of epidermal dedifferentiation during wound healing and limb regeneration in the axolotl (*Ambystoma mexicanum*). *Dev Biol* 2008;319:321–335.
- 52** Scimone ML, Lapan SW, Reddien PW. A forkhead transcription factor is wound-induced at the planarian midline and required for anterior pole regeneration. *PLoS Genet* 2014;10:e1003999.
- 53** Tatin F, Taddei A, Weston A et al. Planar cell polarity protein *Celsr1* regulates endothelial adherens junctions and directed cell rearrangements during valve morphogenesis. *Dev Cell* 2013;26:31–44.
- 54** Tissir F, Goffinet AM. Shaping the nervous system: Role of the core planar cell polarity genes. *Nat Rev Neurosci* 2013;14:525–535.



See [www.StemCells.com](http://www.StemCells.com) for supporting information available online.